ROYAL SOCIETY
OF CHEMISTRY

PAPER
Jörg Feldmann *et al.*
AF₄-MALS-SP ICP-ToF-MS analysis gives insight into nature
of HgSe nanoparticles formed by cetaceans

Environmental Science Nano

PAPER

Check for updates

AF₄-MALS-SP ICP-ToF-MS analysis gives insight into nature of HgSe nanoparticles formed by cetaceans†

Lhiam Paton, [iD] [a] Thebny Thaíse Moro,[abc] Thomas Lockwood,[d] Tatiane de Andrade Maranhão,[b] Gerhard Gössler,[e] David Clases [iD] [c] and Jörg Feldmann*[a]

Cetaceans are known to accumulate very high levels of mercury (Hg) and unlike fish species, most of the mercury is not present as methylmercury (MeHg) but instead as inorganic Hg. It has been suggested this is a result of a detoxification process which involves the sequestering of Hg by Se-containing proteins, concluding with the formation of HgSe nanoparticles. However, their elemental compositions besides Hg and Se, as well as their genesis are unknown. We applied asymmetric flow-field flow fractionation-multiangle laser light scattering (AF₄-MALS) coupled to single particle inductively coupled plasma-time of flight-mass spectrometry (SP ICP-ToF-MS) for the size-dependant separation, counting and further elemental characterisation of Hg/Se-containing nanoparticles in the liver and cerebellum of a sperm whale. Using a proteinase K digestion method, we isolated and identified particles which had size-independent masses of Hg and as well as a continuous molar ratio of Hg to Se. We also identified Cd and Sn on particles alongside Hg and Se, which indicated the detoxification process resulting in Hg/Se nanoparticles may not be specific to MeHg. This data indicates nanoclusters of toxic elements, bound to selenium, make up a nanoparticle core which is surrounded by a larger non-metal(loid) corona.

Environmental significance

Methylmercury (MeHg) is a potent neurotoxic which bioaccumulates throughout the marine food web. MeHg concentrations in marine organisms are frequently found in the mg kg⁻¹ range. However, cetaceans show an extraordinary capability to demethylate a large percentage of this toxic species and it has been suggested that this results in HgSe nanoparticle formation. It is necessary to probe further into this phenomenon to better understand a critical endpoint in the bioaccumulation of Hg and potentially shed light on the importance of Se, not only for Hg but also, for other toxic elements and the subsequent impact this process has on the lifecycle of cetaceans.

Introduction

Mercury (Hg) accumulates through trophic levels leading to high concentrations in major organs of predatory animals.[1] As such, whales as an animal at the top of their food chain are exposed to Hg in high concentrations through their diet and this results in a considerable accumulation of Hg in their major organs.[2,3] For pilot whales, it was previously shown that Hg accumulates with age and that concentrations may exceed 500 mg Hg per kg in the liver.[2,4] Dietary sources are the main contributors for Hg, which for predatory whales typically consists of squid and a variety of fish.[5] Ingested MeHg is partially metabolised in a demethylation step as a protective mechanism to shield organs from potentially severe toxic effects associated with high MeHg levels. Following demethylation, Hg was suggested to bind Lewis soft Se bases present in larger selenoenzymes[6] to form inert HgSe (tiemannite) nanostructures.[7–9] Nano and micro-sized HgSe crystals have been identified by several different analytical techniques and in a wide range of organs and tissues of cetaceans including brain, liver, kidney, muscle, and spleen.[4,10–13] Mapping with synchrotron-XRF showed the co-location of Hg with Se and determined a median molar ratio (0.7 : 1) of mercury to selenium. Analysis of the same pilot whale samples by

a Trace Element Speciation Laboratory (TESLA), Institute for Analytical Chemistry, University of Graz, 8010 Graz, Austria. E-mail: joerg.feldmann@uni-graz.at
b Departamento de Química, Campus Trindade, Universidade Federal de Santa Catarina, Florianópolis, 88040-900, SC, Brazil
c ηµLab, Institute for Analytical Chemistry, University of Graz, 8010 Graz, Austria
d Hyphenated Mass Spectrometry Laboratory, University of Technology Sydney, 2007 Sydney, Australia
e ACHE, Institute for Analytical Chemistry, University of Graz, 8010 Graz, Austria
† Electronic supplementary information (ESI) available. See DOI: https://doi.org/10.1039/d3en00886j

X-ray absorption near edge structure (XANES) spectroscopy[4] found that HgSe was present in whale tissues of older individuals while in juvenile whales there was no evidence for HgSe. It is still unclear how these particles are formed, which cells are responsible and to what extent these nano- or microparticles are composed of tiemannite. Further characterisation of these particles is necessary and especially recent advances in single particle analysis (SP) via inductively coupled plasma-mass spectrometry (ICP-MS) have the potential to shed light on these particles, their sizes, number concentrations and compositions.

SP ICP-MS involves the analysis of dilute particle suspensions leading to the ionisation of individual particles in plasma and the formation of spatially separated ion clouds. These ion clouds consisting of singly charged elemental cations are subsequently sampled from the plasma and analysed in individual pulses. In conjunction with standards, models on particle size and mass distributions can be established. In the past, SP ICP-MS was employed to inquire the size of particles in whales returning largest particles in old whales, which interestingly also exhibited varying Hg isotopic ratios depending on age and on tissue type.[7,9] A game changer for the study of elemental compositions in single particles was the maturation of time-of-flight mass analysers for ICP-MS (ICP-ToF-MS). Whilst quadrupoles as most frequently applied mass analyser in ICP-MS can only monitor one isotope at a time, ToF analysers enable the simultaneous acquisition of whole elemental mass spectra and therefore promotes the investigation of particle stoichiometry and non-target particle screenings. However, it is worth emphasising that SP ICP-ToF-MS only considers elements in single particles if their mass is above a certain decision limit which is stipulated by the ionic background and instrumental properties (e.g., sensitivity, noise). As such, SP ICP-ToF-MS is unable to measure elements which may constitute large fractions of the particle including C, N, O, H and S. This is particularly problematic when trying to model size distributions and calls for complementary techniques to assess particle sizes. This can for example be achieved by coupling asymmetric flow-field flow fractionation multiangle laser light scattering (AF$_4$-MALS) to SP ICP-ToF-MS which can provide additional and complementary perspectives on particle composition and size. Previously, AF$_4$-MALS-SP ICP-ToF-MS has been applied to investigate individual cells[14] and engineered metallic nanoparticles[15] and has the capability to provide new insights into the Hg metabolism of cetaceans.

The aim of this study is to demonstrate the capabilities of SP ICP-ToF-MS for the detection and characterisation of naturally formed inorganic nanoparticles containing both Se and Hg. We developed and tested two different tissue digestion approaches to recover particles from whale tissues and applied SP ICP-ToF-MS as well as AF$_4$-MALS-ICP-ToF-MS (with and without single particle analysis) to characterise sizes, masses, and elemental compositions of particles.

Methods

Whale sampling

The Scottish Marine Animal Stranding Scheme (SMASS) sourced samples of liver tissues from a sperm whale (Physeter macrocephalus). The sub-adult (exact age unknown) male sperm whale was stranded and sampled at Ardersier, Scotland (latitude: 57.562, longitude: −4.0419, date: 06.01.20). By visiting the SMASS website (Scottish Marine Animals Stranding Scheme: https://stranding.org accessed 21.02.23) website it is possible to see information, such as autopsy results, for all strandings which occur across Scotland. The sampling of 21 pilot whales (Globicephala melas), that were stranded on a beach between Anstruther (latitude 56.22298, longitude: −2.700539) and Pittenweem (latitude 56.214, longitude: −2.732285), Scotland in 2012, was further detailed in a previous study.[2]

Nanoparticle extraction for SP ICP-ToF-MS of whale samples

Two extraction methods were tested to recover single particles from whale tissues: first, an enzymatic digestion, which has been reported previously for HgSe particle extraction,[4] and second, a water extraction. The enzymatic digest used 20 mg of dry whale liver tissue which was incubated overnight at 37 °C in a solution of 1 mg mL^{-1} proteinase K (Merck, Austria) and 5 mg mL^{-1} sodium dodecyl sulphate (Merck, Austria). The solution was buffered to pH 7.4 with 50 mM ammonium bicarbonate (Merck, Austria) and finally diluted in MilliQ (18.2 MΩ cm, Millipore) for analysis. For water-based extraction, 20 mg of whale liver tissue was incubated overnight at 15 degrees in a solution of 5 mg mL^{-1} SDS prepared in MilliQ water. The samples were vortexed for 15 seconds before incubation. The enzymatic digest was used as the primary method as it liberated the highest number of particles.

AF$_4$-MALS-ICP-MS/MS

An asymmetric flow field-flow fractionation system (AF$_4$, Postnova, Landsberg, Germany) equipped with an analytical channel containing a 350 μm spacer and 10 kDa regenerated cellulose membrane was coupled to a multiangle laser light scattering detector (MALS, Postnova, Landsberg, Germany). 0.2% Novachem solution was prepared in MilliQ (v/v) and used as mobile phases for all analyses. Channel pressure was maintained between 7.5 and 8.5 bar throughout all measurements.

A latex nanoparticle standard mixture (Nanosphere, Thermo Scientific, UK) containing spherical particles with diameters: 60, 125 and 350 nm were separated using the fractionation method optimised for the whale sample (Fig. S1†) and the MALS signal was normalised to the 125 nm particle. Analysis by MALS returns a radius of gyration (r_g) which, for the case of a spherical particle, can be related to the geometric radius (r_{geo}). The ratio between r_g and r_{geo} for a spherical particle (labelled α) is 0.775, meaning the geometric

1884 | Environ. Sci.: Nano, 2024, 11, 1883–1890

This journal is © The Royal Society of Chemistry 2024

radius can be calculated from eqn (1). We do not know the exact shape of these naturally occurring compounds, we assumed the particles were spherical. An extract from the MALS signal is shown in Fig. S2.†

$$r_{geo} = \frac{r_g}{\alpha} \qquad (1)$$

The AF$_4$-MALS system was initially coupled to an Agilent 8900 ICP-MS/MS (Agilent Technologies, USA) instrument. ^{202}Hg was analysed on-mass and ^{80}Se was analysed with an oxygen-mass shift at m/z 96 as ^{80}Se^{16}O. The determination of elemental recoveries was performed by analysing element standards for ICP-MS in a flow-injection approach according to approaches reported previously for AF$_4$-ICP-MS for NP analysis and specifically for the analysis of Hg and Se NPs.[16,17] The AF$_4$ channel recovery percentages for Hg and Se were 126% and 106%, respectively, and were calculated by determining the ratio of the concentration of the target element in a sample which was passed through the channel of the AF$_4$ but experienced no cross flow (tip flow = 0.5 mL min^{-1}, focus flow = 0 mL min^{-1}, cross flow = 0 mL min^{-1}) to the concentration of the target element in a sample which was fractionated using the method described in Fig. S1.†

AF$_4$-MALS-ICP-ToF-MS

A Vitesse-series ICP-ToF-MS instrument (Nu Instruments, Wrexham, UK) was coupled online to the AF$_4$-MALS system described above. For AF$_4$-MALS-SP ICP-ToF-MS analysis, a 10 µg L^{-1} mixed ionic standard solution was measured to determine the response (counts/µg L^{-1}) and the sample uptake rate was determined gravimetrically. For the determination of the transport efficiency, 100 nm gold nanoparticles (NanoComposix) and a 10 µg L^{-1} ionic gold standard solution were measured and yielded 3.5% (size method). The dwell time for all analyses was 0.096 ms and four spectra were binned before saving data to disk. Data analysis was performed on an ToF-ready version (V1.1.2) of the data processing platform SPCal.[18] Compound Poisson statistics were used to set a decision limit ($\alpha = 10^{-6}$), over which a signal was considered a particle. Single particle signals were then accumulated over the decision limit and calibrated as described elsewhere.[18] ICP-ToF-MS instrumental parameters were as follows: RF power = 1000 W, coolant gas flow = 13 L min^{-1}, auxiliary gas flow = 1000 mL min^{-1}, nebuliser gas flow = 1130 mL min^{-1}.

Statistics

Statistical comparison of slopes generated from plotting Hg mass against Se mass for particles with different retention times was done in R (code used: Fig. S3†) with a bootstrap approach. The bootstrap approach was chosen because it was not possible to compare the slopes using the standard approach based on linear regression, *i.e.*, testing for differences in slopes by including an interaction term in the regression model. Linear regression could not be used due to violation of basic model assumptions. In this case, neither homoscedasticity nor normally distribution of errors could be assumed. Since there was plenty of data available, these data sets have been well suited for bootstrap-based methods that, unlike simple linear regression, do not rely on distributional assumptions.

The statistical test for comparing the slopes with respect to two different datasets was based on the following approach: the number of bootstrap iterations was set to 10^4. Next, there were 10^4 bootstrap replicates generated by resampling with replacement from each data set. Each bootstrap replicate was the same size as the original dataset, and each observation could be selected more than once or not at all when such a replicate was formed, as observations were selected with replacement. For each of these replicates, the slope was determined and the difference between these slopes was calculated and stored in each iteration. Therefore, for the comparison of two different data sets with respect to slopes, 10^4 of such bootstrap differences in slopes were calculated. Finally, since a two-sided comparison of the slopes was performed, *i.e.*, the hypotheses.

$$H_0\text{: slopes are equal } vs. \ H_1\text{: slopes are not equal.}$$

were tested, the p-value was calculated as (# = number of)

$$p\text{-value} = \frac{2 \ \min \ (\# \text{ slope differences} > 0, \ \# \text{ slope differences} \leq 0)}{\# \text{ bootstrap iterations}}. \qquad (2)$$

The validity of this approach was investigated in a simulation study with artificial data satisfying the assumptions of linear regression. Comparing the performance of the bootstrap-based test with the results obtained based on linear regression yielded similar results in this case.

Results and discussion

AF$_4$-MALS-ICP-MS/MS

For initial assessments of particle fractions and their association with Hg and Se, AF$_4$-MALS was used in conjunction with ICP-MS/MS. An AF$_4$ method was developed to separate particle sizes in a range of 1–1000 nm and extractants from sperm whale liver were analysed. The results are shown in Fig. 1 indicating four distinguishable regions present in the MALS channel. The signal at 10 min corresponded to small particles (focusing segment) with sizes below 60 nm in size. The other signal regions were located 12–20 (fraction A), 20–37.5 (fraction B) and 40–50 minutes (fraction C). For fraction A, a radius of gyration (r_g) of 80 nm was determined, assuming a spherical particle shape, a geometric diameter of approximately 200 nm. For the final two fractions (B and C) it was possible to identify particles
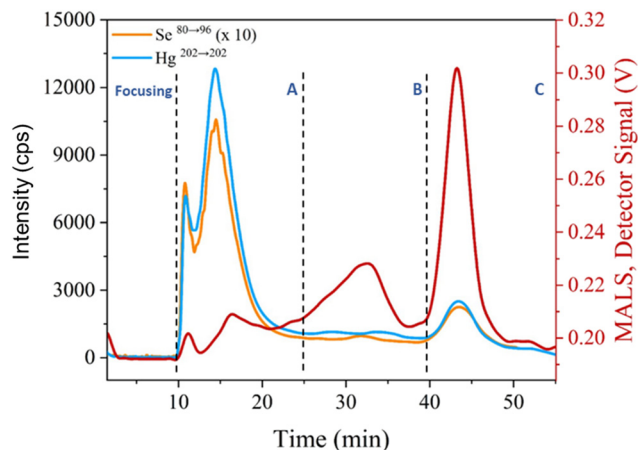
This journal is © The Royal Society of Chemistry 2024

Environ. Sci.: Nano, 2024, **11**, 1883–1890 | **1885**

Fig. 1 AF$_4$-MALS-ICP-MS/MS analysis of a whale liver digest. The MALS signal is shown in red, while the blue and orange signals represent Hg and Se as detected by ICP-MS/MS. The figure is segmented into four sections by black dotted lines, the produced sections denote: focusing step, fraction A (10–25 minutes), fraction B (25–40 minutes), and fraction C (40–55 minutes).

with estimated diameters of 300 and 770 nm, respectively. While these estimations require the assumption of a spherical particle, two additional experiments suggested that the estimations are reasonable. Fig. S4† shows that a latex particle mixture was separated by the method used for the whale sample and that spiking of the latex sample with increasing volumes of whale digest led to the particles eluting sooner. The result is the 60 and 125 nm co-eluting, within fraction A, and the 350 nm particle being separated, now eluting in fraction B, and in the whale sample the largest particles elute after the cross flow had reached zero. Secondly, filtering prior to analysis with a 220 nm filter saw the second half of the fractogram showed no signal, cutting off particle sizes where estimates of 300 nm or larger were made. The formation of Hg/Se containing particles with high

variation in size in the livers of cetaceans is known and has been discussed previously in the literature.[4] Using ICP-MS/MS as additional detector for AF$_4$ enabled the determination of Hg and Se throughout the fractionation process as shown in Fig. 1 and indicated a co-elution of Hg and Se in fractions A and C. However, a continuous signal was detected during the elution of fraction B and suggested the presence of both Hg and Se. Consequently, the range of particle sizes produced within the whale tissues ranged between 200 nm (fraction A) and 770 nm (fraction C) but particles were detectable throughout this size range, which was from polydisperse natural particles.

SP ICP-ToF-MS

Following the identification of Hg and Se particles in extracts by AF$_4$-MALS-ICP-MS/MS, the extracts were analysed using SP ICP-ToF-MS to prove the association of Hg and Se on a single particle basis. While in previous study imaging methods confirmed the colocalization of Hg and Se in investigated sample areas, SP analysis additionally proved the presence of discrete particles. Due to the acquisition of full mass spectra for each data point, correlations to other metals could be investigated additionally. The found composition of particles is illustrated in Fig. 2. Besides Hg and Se, Cd was detected, Fig. 2A shows the transient data recorded in SP ICP-ToF-MS indicating the SP signals for Hg, Se, and Cd. Fig. 2B shows a selected particle signal indicating the simultaneous detection of all three elements in one composite particle. 1029 particles per min were detected containing Se and Hg and 145 particle per min additionally contained Cd above the lower mass detection limit (mDL). Particle number concentrations in both liver and cerebellum tissues were determined to be 7.4×10^{10} Hg/Se particles per g and 7.8×10^{9} Hg/Se particles per g, respectively. In liver, the mean molar ratio of Hg : Se ratio was found to be 0.84 ± 0.05 ($n = 3$, method triplicate) and in the
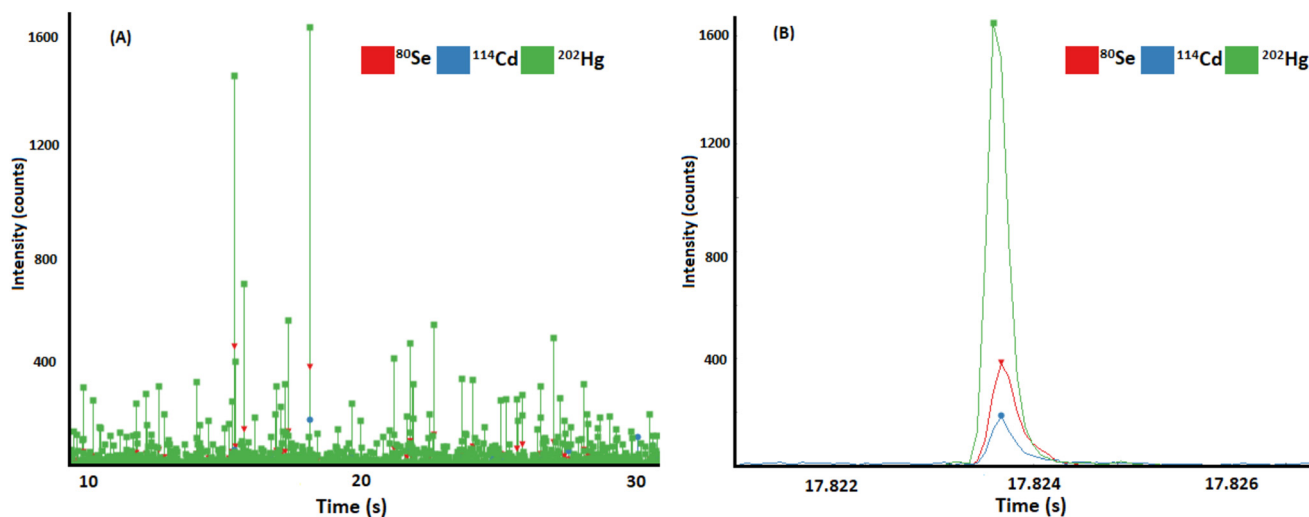

Fig. 2 (A) Shows an example of the data produced from SP ICP-ToF-MS analysis of enzymatically digested sperm whale liver, where Hg, Se and Cd can be found. (B) Shows an example of a particle containing Hg, Se, and Cd.
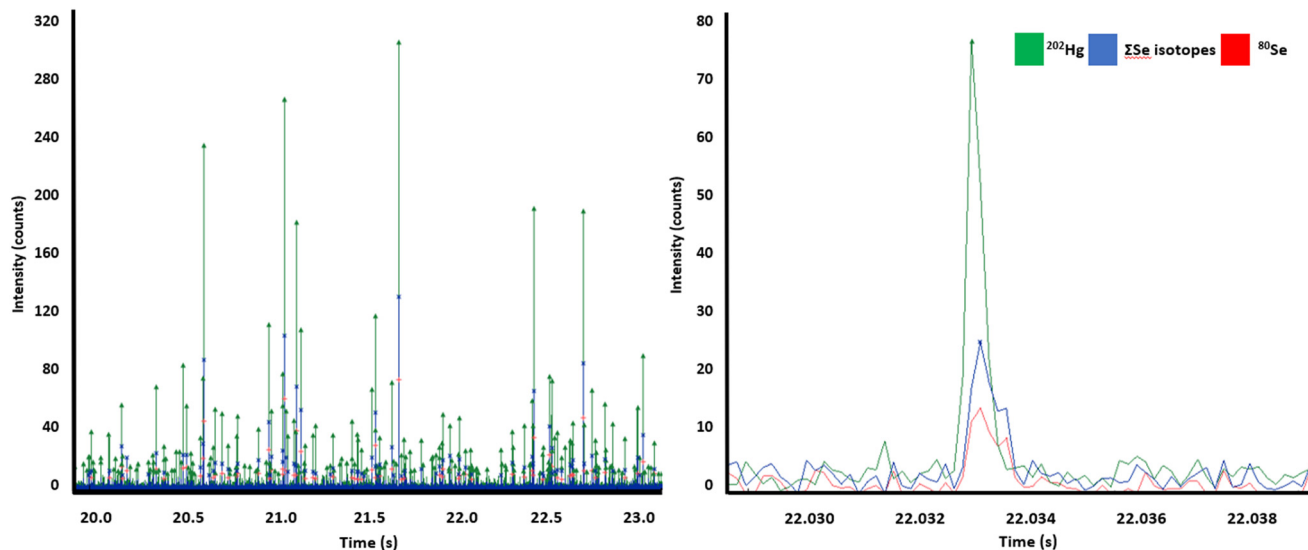
Fig. 3 The improvement of signal intensity when adding up all available isotopes of an element, like Se, is shown here. (Left) Hg/Se particles identified in a sperm whale liver sample. (Right) Shows the introduction of the sum of all Se isotopes, compared to the most abundant isotope (^{80}Se). With this introduction comes the identification of a Hg/Se particle which would not have otherwise been identified as the signal for ^{80}Se fell below the detection threshold.

cerebellum duplicate measurements found Hg : Se atomic ratio of 0.73 and 0.84. The ratios calculated here are comparable with the molar ratio of Hg : Se determined previously by XRF.[4] Nevertheless, it was a possibility that the sample treatment could have an impact on particle integrity and determined elemental ratios on extracted particles may be a result of an artifact generated in sample preparation. As such, results obtained in SP analysis were compared against synchrotron-based XRF-data obtained by our group previously.[2,4] This confirmed that the atomic Hg : Se ratios on the extracted NPs were unaffected by the proteinase K digestion (Fig. S5†).[4] Considering the sample preparation, with an appropriately large sample mass (20 mg) the Hg/Se particles appeared to be evenly distributed throughout the whale tissue, however, it has previously been shown by NanoSIMS that when considering the micrometre scale, or below, the Hg/Se in the whale tissue is found in hotspots and is heterogeneously distributed. This has also been visible when LA-ICP-MS and XRF were applied for whale tissue analysis.[4,13]

The correlation between Hg and Se in marine organisms has been discussed for many years[19,20] and it is established that Se plays an essential role in limiting methylmercury-induced toxicity in mammals.[8] It has been proposed that this is achieved by sequestering inorganic mercury, which at some stage must have been formed from demethylation of methylmercury, as inert tiemannite nanoparticles which form in the major organs of cetaceans. To date, this process has not been identified in fish as methylmercury appears to continue to accumulate linearly with age.[21]

The simultaneous acquisition of isotopes/elements in ToF in a single particle is a crucial advantage to decipher the heavy metal metabolism in cetaceans, although, relative to a quadrupole the sensitivity is lower. To overcome the reduced sensitivity and promote the analysis of small and

heterogeneous particles, we followed two strategies to improve sensitivity and ToF duty cycle as presented in a recent study.[22] Firstly, we limited the mass range to 74–204 amu which enabled a higher duty cycle and therefore higher counting rates and sensitivities. Secondly, we used a post-analysis algorithm which summed up all isotopes of Se, Hg and Cd for increased signal to noise ratios. Fig. 3 highlights this process, Fig. 3A shows an example of data for particles containing both Hg and Se. Fig. 3B shows from the same data set an example of a Hg/Se containing particle which was only identifiable by the summing of isotopes (blue line), as the signal for the most abundant Se isotope (red line) was not high enough to reach the detection threshold. This approach increased the particle count by factor 1.5 and the mass limit of detection (mLOD) for this analysis dropped from 0.17 fg for Se^{80} to 0.12 fg for the sum of Se isotopes. For Hg and Cd, the mLOD improved from 0.16 fg (^{202}Hg) to 0.09 ($\sum$Hg) and from 0.06 fg to 0.04 fg ($\sum^{106}$Cd ^{108}Cd, ^{110}Cd, ^{111}Cd, ^{113}Cd). In total 145 Cd/Hg/Se particles per min were detected. The atomic ratios of Cd to Se and Hg in single particles was found to be approximately 7.8 : 1 (Hg : Cd) and 9.8 : 1 (Se : Cd), respectively. Overall, Cd made up the smallest mass fraction of all detected particles.

Besides Cd, some Hg-particles further incorporated Sn as shown in Fig. 4. To avoid misinterpretation through isotopic interferences, correlations were only considered between the isotopes of Cd (Cd^{106}, Cd^{108}, Cd^{110}, Cd^{111} and Cd^{113}) and Sn (Sn^{117}, Sn^{118}, Sn^{120}, Sn^{122} and Sn^{124}). So far, it was not possible to directly identify Se and Sn on the same particle, which may be a result from relatively high detection limits for Se and a rare incidence of Sn particles, which had no spectral overlap. For particles containing both Cd and Sn, Sn masses greatly exceeded those of Cd by between 50 and 300 times. This identification of other non-essential elements
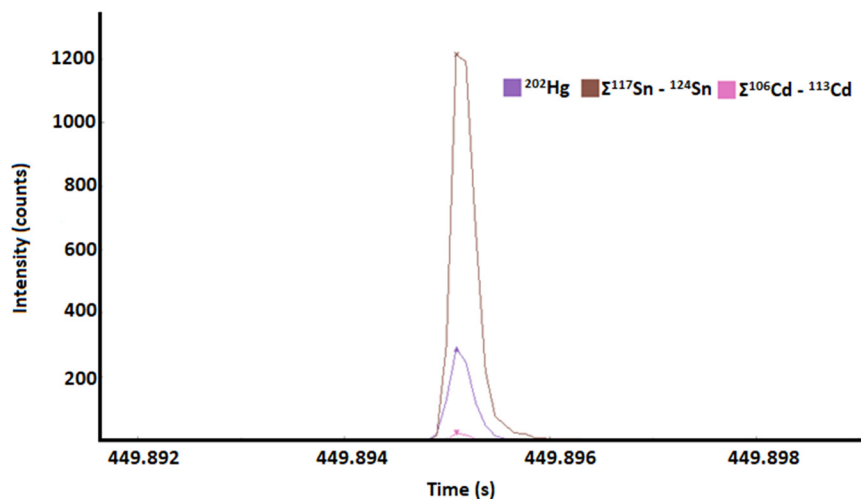
Fig. 4 An example is given of Hg, Cd and Sn all being found on single particle in the enzymatically digested sperm whale liver sample. Benefitted by post-analysis isotope accumulation for Sn and Cd.

(Cd, Sn) in the same particles as Hg (Fig. 4) may suggest that the process which results in Hg being bound to Se in whale organs is also important for the sequestering of other elements which could otherwise be toxic, such as, Cd and Sn.[23] The interactions of Hg and Cd with Se have been discussed in the literature[2,24,25] and it was established that both Cd and Hg can bind to Se and can cross the blood–brain barrier.[2] So far, there is no information on how the transport of these elements is influenced by the presence or formation of particulate structure.

AF$_4$-MALS-SP ICP-ToF-MS

Following the individual application of AF$_4$-MALS-ICP-MS/MS and SP ICP-ToF-MS, AF$_4$-MALS-SP ICP-ToF-MS was used concurrently to investigate its utility to characterise extracted and size-separated particles further. The coupling of these techniques provides a range of complementary insights on extracted particles and allows the deduction of a large range of information including particle size, compositions, number concentration (PNC) and therefore allows to correlate different parameters such as size and composition. Enzymatic digests of sperm whale liver were prepared and measured by SP ICP-ToF-MS in triplicate and returned an average Hg : Se ratio of 0.84 : 1. For AF$_4$-SP ICP-ToF-MS analysis, one digest was selected and further characterised. It was hypothesised that particle stoichiometry would vary across different size ranges: with larger particles expected to elute later and contain higher masses of Hg and Se relative to smaller, earlier eluting particles. Across the fractionation process 4163 Hg/Se particles were detected and Table 1 shows that these particles can be found throughout the fractionation process, as expected from Fig. 1, and that the greatest number of particles is found where particle size is highest. Interestingly, it is also apparent that with increasing particle sizes, particle-based Hg : Se ratios did not increase linearly as the ratio went from 0.80 : 1 to 0.84 : 1 between

Table 1 Data from AF$_4$-MALS-SP ICP-ToF-MS measurement of sperm whale liver, showing particle count of Hg and Se detected and the ratios in which they are present relative to each other on the HgSe particles detected. Data processed in open access software created by Lockwood et al.[18] (version: spcal_1.1.2) Hg$_{mLOD}$ = 0.09 fg, Se$_{mLOD}$ = 0.12 fg. Segment titles (A–C) can be compared to the fractogram shown in Fig. 1

Segment (Fig. 1)	Time (min)	HgSe particles	Hg : Se
A	10–25	73	0.80 : 1
B	25–40	1250	0.84 : 1
C	40–55	3685	0.82 : 1

fraction A and B, before dropping again to 0.82 : 1 in fraction C where the greatest number of particles were found and where the largest particles were detected. We repeated this experiment with a simplified sample preparation, without proteinase K, using only water and 5 mg mL^{-1} SDS to promote particle stabilisation. SP ICP-ToF-MS analysis of the water extracts found a Hg : Se molar ratio of 0.6 : 1. Following this with AF$_4$-MALS-SP ICP-ToF-MS again showed that fractionation of Hg/Se particles of increasing sizes was possible (Fig. S6†) and that the molar ratio of Hg : Se across the analysis was maintained (0.59 : 1, 0.55 : 1 and 0.56 : 1 in the recorded 15-minute segments from 10–55 minutes). The water extract did produce the lowest Hg : Se atomic ratio across all sperm whale analyses (cerebellum ≈ 0.8 : 1, liver ≈ 0.8 : 1), therefore, in terms of extraction efficiency, it would appear the proteinase K digest was capable to liberate more particles which have higher Hg mass and which may still be bound to Se-proteins in the tissue. So, the fractionation of HgSe particles by size is still possible without enzymatic extraction, suggesting that the different particle sizes are not generated by the digest. These Hg : Se ratios were determined by consideration of the slope obtained when plotting the mass of Hg against the mass of Se for particles containing both (Fig. S7†). The total number of particle events increased throughout the fractogram and with this the number of Hg/Se-containing particles. However, there was no evidence that

1888 | *Environ. Sci.: Nano*, 2024, **11**, 1883–1890

This journal is © The Royal Society of Chemistry 2024

the mass of these elements is correlated with the size of the particles. Statistical comparison of the slopes using a bootstrap approach returning p-values > 0.05 in all cases; these are summarised in Table 2, the resulting figure showing all data points and slopes overlain is shown in Fig. 5. The maintenance of the molar ratio between Hg and Se is unlikely to be a result of several smaller particles agglomerating as it was visible when reducing the analysis window to 5 minute sub-fractions that the Hg mass did not increase throughout the fractionation process (Table S1†). Similarly, increasing particle size is not likely to be an artifact generated from using SDS, which is used to improve particle stability, as monitoring of sulphur by AF$_4$-MALS-ICP-MS/MS

Table 2 Statistical comparisons of the slopes generated when plotting Hg mass *vs.* Se mass (left hand side column compared with central column returns the p-value) for each fraction of the AF$_4$-MALS-SP ICP-ToF-MS analysis is shown. In each case the slopes were found not to be statistically different. Confirming that the Hg:Se ratio was unchanged with respect to increasing particle size

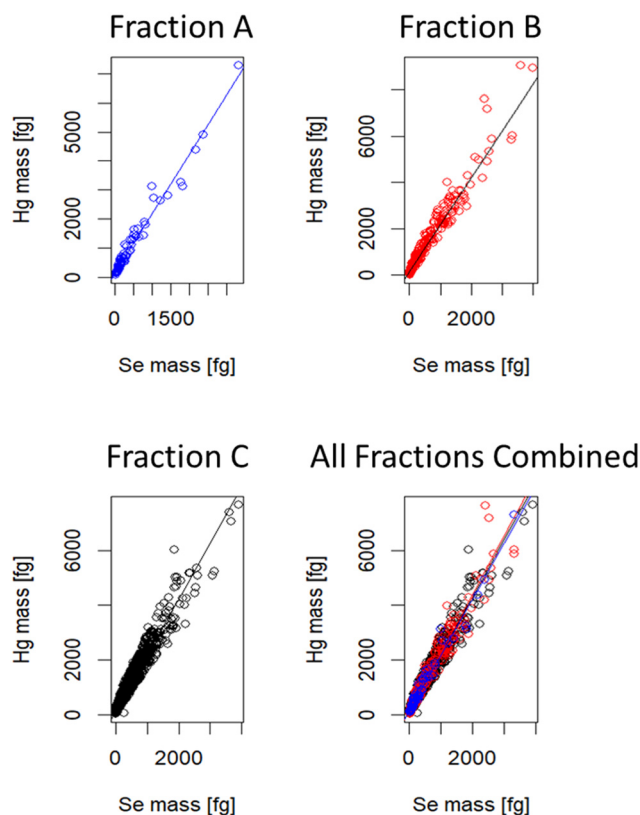| Fraction	Fraction	p-Value
A	B	0.27
A	C	0.45
B	C	0.50

Fig. 5 Shown are comparisons of the three slopes generated from plotting Hg mass *vs.* Se mass on particles which were separated by AF$_4$ and analysed by SP ICP-ToF-MS. The fourth plot shows all data combined with the three slopes also overlain, highlighting the similarity in the behaviour which is independent of particles size.

found the sulphur was not present in the fractions containing the largest particles (Fig. S8†).

We suggest that the Hg/Se particles which have been discussed as the endpoint of MeHg detoxification are not solely composed of Hg and Se but incorporate other metals (Cd, Sn) and based on the data from AF$_4$-MALS-SP ICP-ToF-MS, it is likely that a significant portion of the structure is non-metal or metalloid (*i.e.*, biomolecules forming a corona around a metal core). Although the differences in particles size are not clearly correlated with the mass of Hg or the atomic ratio of Hg:Se on the particles, it is possible that the sizes are indicative of differences in the particles, or perhaps this is because of differences in the cells which the Hg/Se are stored in, which would be destroyed by the freeze-drying process, liberating the particles but leading to differences in the chemistry of the particles themselves.[16]

Conclusion

This study demonstrates the first successful coupling of AF$_4$ to ICP-ToF-MS in single particle mode and realised the detection of individual Hg/Se nanoparticles extracted from sperm whale tissues. By studying elemental composition on a single particle level, it was further possible to pinpoint other elements to be associated with Hg-containing particles such as Cd and Sn. This suggests that the endpoint of MeHg detoxification is not solely the formation of Hg/Se nanoparticles but composite nanoparticles that include other toxic elements and not just Hg. Hyphenating AF$_4$-MALS and SP ICP-ToF-MS provided evidence that Hg/Se-containing particles present in sperm whale liver extracts existed in a range of different sizes from approximately 200–770 nm. In each case the increasing size of the particles was not found to be directly correlated to the mass of Hg present in the fractionated particles nor did increasing particle size have an impact on the molar ratio identified between Hg and Se on the particles. The potential for this result to be an artifact of sample preparation was investigated by changing the sample preparation conditions, probing the possible impact of SDS on particle size and by comparison of previously published XRF data with SP ICP-ToF-MS data. All of which suggest that the size-dependent fractionation is representative of a biological process rather than a sample preparation artifact.

It is possible that the visible fractionation of Hg/Se particles may be a result of different surface properties of the particles, potentially due to more than one cell type being involved in the process, leading to interactions with different reactive, non-protein, biomolecules. Although the identification of these biomolecules would be a fundamental next step required to support this hypothesis. Nevertheless, Hg/Se nanoparticles were identified at a range of sizes on the nanometre scale and that the entire composition of the particle cannot be explained by metals and Se-proteins. The next step in deciphering the detoxification pathway which results in nanostructure formation should consider the cells which are responsible for the transformation and storage of Hg/Se-containing particles. The

This journal is © The Royal Society of Chemistry 2024

Environ. Sci.: Nano, 2024, **11**, 1883–1890 | **1889**

best approach would likely take advantage of nanoscale imaging techniques for the simultaneous identification of cells and elemental distribution.

Author contributions

LP was involved concept development, analytical method development, analysis, data interpretation, manuscript writing and editing. TTM provided support in method development, sample preparation, analysis, and manuscript editing. TL developed data analysis software used, manuscript editing. GG performed statistical analysis, manuscript writing and editing. TAM provided TTM supervision and manuscript editing. DC provided spICP-ToF-MS expertise and support, concept development, method development, manuscript writing and editing. JF conceptualisation, concept development, manuscript writing and editing.

Conflicts of interest

There are no conflicts to declare.

Acknowledgements

References

1 R. A. Lavoie, T. D. Jardine, M. M. Chumchal, K. A. Kidd and L. M. Campbell, *Environ. Sci. Technol.*, 2013, **47**, 13385–13394.

2 Z. Gajdosechova, A. Brownlow, N. T. Cottin, M. Fernandes, F. L. Read, D. S. Urgast, A. Raab, J. Feldmann and E. M. Krupp, *Sci. Total Environ.*, 2016, **545–546**, 407–413.

3 W. F. Fitzgerald, C. H. Lamborg and C. R. Hammerschmidt, *Chem. Rev.*, 2007, **107**, 641–662.

4 Z. Gajdosechova, M. M. Lawan, D. S. Urgast, A. Raab, K. G. Scheckel, E. Lombi, P. M. Kopittke, K. Loeschner, E. H. Larsen, G. Woods, A. Brownlow, F. L. Read, J. Feldmann and E. M. Krupp, *Sci. Rep.*, 2016, **6**, 34361.

5 M. B. Santos, S. S. Monteiro, J. V. Vingada, M. Ferreira, A. López, J. A. Martínez Cedeira, R. J. Reid, A. Brownlow and G. J. Pierce, *Mar. Mammal Sci.*, 2014, **30**, 1–19.

6 M. B. Romero, P. Polizzi, L. Chiodi, K. Das and M. Gerpe, *Mar. Pollut. Bull.*, 2016, **109**, 650–654.

7 Z. Gajdosechova, Z. Mester, J. Feldmann and E. M. Krupp, *TrAC, Trends Anal. Chem.*, 2018, **104**, 95–109.

8 N. V. C. Ralston and L. J. Raymond, *Toxicology*, 2010, **278**, 112–123.

9 E. Bolea-Fernandez, A. Rua-Ibarz, E. M. Krupp, J. Feldmann and F. Vanhaecke, *Sci. Rep.*, 2019, **9**, 7262.

10 E. Nakazawa, T. Ikemoto, A. Hokura, Y. Terada, T. Kunito, S. Tanabe and I. Nakai, in *Metallomics*, 2011, pp. 719–725.

11 M. Marumoto, M. Sakamoto, M. Nakamura, K. Marumoto and S. Tsuruta, *Acta Vet. Scand.*, 2022, **64**, 1.

12 F. E. Huggins, S. A. Raverty, O. S. Nielsen, N. E. Sharp, J. D. Robertson and N. V. C. Ralston, *Environ. Bioindic.*, 2009, **4**, 291–302.

13 M. A. Subirana, L. Paton, J. Hall, A. Brownlow, E. M. Krupp, J. Feldmann and D. Schaumlöffel, *Anal. Chem.*, 2021, **93**, 12733–12739.

14 M. I. Chronakis, M. von der Au and B. Meermann, *J. Anal. At. Spectrom.*, 2022, **37**, 2691–2700.

15 O. Meili-Borovinskaya, F. Meier, R. Drexel, M. Baalousha, L. Flamigni, A. Hegetschweiler and T. Kraus, *J. Chromatogr. A*, 2021, **1641**, 461981.

16 D. Ruhland, K. Nwoko, M. Perez, J. Feldmann and E. M. Krupp, *Anal. Chem.*, 2019, **91**, 1164–1170.

17 K. C. Nwoko, X. Liang, M. A. Perez, E. Krupp, G. M. Gadd and J. Feldmann, *J. Chromatogr. A*, 2021, **1642**, 1164–1170.

18 T. E. Lockwood, R. Gonzalez De Vega and D. Clases, *J. Anal. At. Spectrom.*, 2021, **36**, 2536–2544.

19 D. Y. Yang, Y. W. Chen, J. M. Gunn and N. Belzile, *Environ. Rev.*, 2008, **16**, 71–92.

20 J. H. Koeman, W. H. Peeters, C. H. Koudstaal-Hol, P. S. Tjioe and J. J. de Goeij, *Nature*, 1973, **245**, 385–386.

21 C.-M. Tseng, S.-J. Ang, Y.-S. Chen, J.-C. Shiao, C. H. Lamborg, X. He and J. R. Reinfelder, *Proc. Natl. Acad. Sci. U. S. A.*, 2021, **118**, 1–6.

22 T. E. Lockwood, R. Gonzalez De Vega, Z. Du, L. Schlatt, X. Xu and D. Clases, *J. Anal. At. Spectrom.*, 2024, **39**, 227–334.

23 A. M. K. Hansen, C. E. Bryan, K. West and B. A. Jensen, *Arch. Environ. Contam. Toxicol.*, 2016, **70**, 75–95.

24 B. J. Wlodarczyk, M. Minta, B. Biernacki and J. Zmudzki, *Pol. J. Environ. Stud.*, 2000, **9**, 323–327.

25 C. Sasakura and K. T. Suzuki, *J. Inorg. Biochem.*, 1998, 159–162.